NIH Public Access
Author Manuscript
*Invest Ophthalmol Vis Sci*. Author manuscript; available in PMC 2013 May 11.

Published in final edited form as:
*Invest Ophthalmol Vis Sci*. 2009 November ; 50(11): 5026–5034. doi:10.1167/iovs.09-3447.

# FoxC1 is essential for vascular basement membrane integrity and hyaloid vessel morphogenesis

**Jonathan M. Skarie** and **Brian A. Link***
Department of Cell Biology, Neurobiology and Anatomy Medical College of Wisconsin, Milwaukee, WI USA

## Abstract

**Purpose—**Alterations in *FOXC1* dosage lead to a spectrum of highly penetrant, ocular anterior segment dysgenesis phenotypes. The most serious outcome is development of glaucoma, but this only occurs in 50–75% of patients. Therefore, the need to identify specific pathways and genes that interact with FOXC1 to promote glaucoma is great. In this study, we investigated loss of *foxC1* in the zebrafish to characterize phenotypes and gene interactions that may impact glaucoma pathogenesis.

**Methods—**Morpholino knockdown in zebrafish, RNA and protein marker analyses, transgenic reporter lines, and angiography, along with histology and transmission electron microscopy were used to study *foxC1* function and gene interactions.

**Results—**Zebrafish *foxC1* genes were expressed dynamically in the developing vasculature and periocular mesenchyme during development. Multiple ocular and vascular defects were found after knockdown of *foxC1*. Defects in the hyaloid vasculature, arterial-venous malformations, and coarctation of the aorta were observed with maximal depletion of *foxC1*. Partial loss of *foxC1* resulted in CNS and ocular hemorrhages, defects in intersegmental vessel patterning, and increased vascular permeability. To investigate the basis for these disruptions, ultrastructure of *foxC1*-depleted hyaloid vascular cells was studied. These experiments, along with Laminin-111 immunoreactivity, revealed disruptions in basement membrane integrity. Finally, co-depletion of *laminin alpha-1* and *foxC1* uncovered a genetic interaction between these genes during development.

**Conclusions—**Genetic interactions between *FOXC1* and basement membrane components influence vascular stability and may impact glaucoma development and increase stroke risk in *FOXC1* patients.

## INTRODUCTION

Gene dosage changes in *FOXC1* result in a spectrum of ocular anterior segment dysgeneses (ASD), including Axenfeld Rieger Anomaly and iridogoniodysgensis.[1–8] All disease forms are developmental, dominantly inherited, and highly penetrant. The most debilitating outcome for ASD patients is the development of glaucoma, which occurs in 50–75% of cases and is often refractive to treatment. [9–11]

Glaucoma is a progressive blinding disease which results from atrophy of the optic nerve and death of retinal ganglion cells. In ASD patients, raised intraocular pressure (IOP) is the greatest risk factor for developing glaucoma.[10] IOP is regulated by aqueous humor flow in the anterior segment of the eye and most typically, elevated IOP is caused by reduced

*Corresponding Author: Brian A. Link, Department of Cell Biology, Neurobiology and Anatomy, Medical College of Wisconsin, 8701 Watertown Plank Rd. BSB 405, Milwaukee, WI 53226, blink@mcw.edu, Phone: 414 456 8072, Fax: 414 456 6517.

NIH-PA Author Manuscript
NIH-PA Author Manuscript
NIH-PA Author Manuscript

NIH-PA Author Manuscript

NIH-PA Author Manuscript

NIH-PA Author Manuscript

aqueous humor drainage. The precise mechanistic relationship between elevated IOP and glaucoma is still unknown. In ASD, development of the outflow structures is compromised, and it is hypothesized that defects in these structures lead to elevated IOP and glaucoma. However, in *FOXC1* disease, it is not understood why glaucoma occurs only in some patients despite the high penetrance of ASD phenotypes.

The role of *FOXC1* in development has been studied in a number of experimental systems including cell culture, mice, zebrafish and frogs. FoxC1 is widely expressed during embryogenesis, but is not ubiquitous. Mice with null *Foxc1* mutations show defects in differentiation of chondrocytes, the renal system, the eyes and vascular system.[2, 12, 13] In addition to null mutations, a hypomorphic allele revealed later developmental requirements of FOXC1.[14] Later on-set defects include cortical dyslamination and skull anomalies. Interestingly, the cortical defects were suggested to be secondary to altered meningeal differentiation. Haploinsufficiency of *Foxc1* in mice has also been used to model human disease. Interestingly, ASD phenotypes were found only in specific mouse strains, while other genetic backgrounds did not show observable defects.[15] These observations reinforce the role of genetic modifiers on *Foxc1*-dependent phenotypes.

A similar distribution of phenotypic defects was found with loss of the closely related gene, *Foxc2*. FOXC1 and FOXC2 share nearly identical DNA binding domains and developmental expression patterns. Compound mutant analysis in mice revealed redundant functions between these factors.[15–18] Vascular phenotypes of *FoxC1/FoxC2* double knockout mice included arterial-venous fate defects and vessel morphogenesis and remodeling anomalies.[17, 19–21] In the zebrafish, *foxC1* is duplicated and there is no evidence for a *foxC2* homolog.[22] However, the combined expression of *foxC1a* and *foxC1b* during zebrafish embryogenesis is similar to that of *FoxC1* and *FoxC2* in higher vertebrates [22, 23], suggesting that zebrafish *foxC1b* is the functional homolog of mammalian *FoxC2*.

In this study, we explore the mechanisms of the eye and vascular phenotypes associated with loss of *foxC1* function in zebrafish. Overall, depletion of *foxC1* resulted in multiple, dose-sensitive vascular phenotypes. In particular, we found that loss of *foxC1* results in defects to vascular basement membrane integrity. These studies provide insight into the mechanisms for how altered FoxC1 function can affect glaucoma and suggest that *FOXC1* mutations in humans may also increase the risk of stroke.

## MATERIALS AND METHODS

### Specimens

Wild-type zebrafish (*Danio rerio*) of the AB/AB and LF/LF backgrounds were reared under standard conditions with a light cycle of 14h light/10h dark. Prior to experimental manipulation or tissue fixation, fish were anesthetized in 0.2 mg per ml of ethyl 3-aminobenzoate methanesulfonate (tricane). All experiments were performed in compliance with the ARVO statement for use of animals in vision research.

### *In situ* Hybridization

Probes against zebrafish *foxC1a (foxC1.1)*, *foxC1b (foxC1.2)*, and *flt4* were produced as previously described.[22, 24] Antisense RNA probes were produced and whole-mount *in situ* hybridization was conducted as previously described.[25, 26] 10–15 embryos, treated with 0.003% phenylthiourea (PTU), were analyzed in each *in situ* experiment. PTU inhibits melanin synthesis. For post-hybridization sectioning, embryos were fixed in 4% paraformaldehyde/PBS and infiltrated with 15% sucrose, 30% sucrose and then 100% Tissue-Tek OCT (Miles Inc., Elkhart, IN, USA). Embryos were oriented in a freezing mold and 10 μm sections were cut on a cryostat and mounted on gelatin-coated glass slides.

NIH-PA Author Manuscript

NIH-PA Author Manuscript

NIH-PA Author Manuscript

### Morpholino Knockdown

Previously described anti-sense morpholinos (MO) used for knockdown were ordered from Gene Tools (Philomath, OR), resuspended in sterile water and injected into 1–4 cell stage embryos. MOs used were (Start codon underlined): *foxC1a* MO2 (GeneID 79374): 5′-CCTGCATGACTGCTCTCCAAAACGG -3′; *foxC1b* MO1 (GeneID 79375): 5′-GCATCGTACCCCTTTCTTCGGTACA-3′ [27]; *laminin alpha-1* MO1 (GeneID 77993333): 5′-ATAAAGCTAAAGCTGTGCTGAAATC-3′ [28, 29] ; Control MO: 5′-CCTCTTACCTCAGTTACAATTTATA-3′. *foxC1a* MO2 and *foxC1b* MO1 were injected together to achieve *foxC1* dMO morphant zebrafish. Other *foxC1* MOs used to verify phenotypes were: *foxC1a* MO1 5′-GTCAAGAAGACTGAAGCAATCCACA -3′; *foxC1b* MO1: 5′-AAGTGAAATGAAGACTATGCAGACG -3′ [27]

### Transmission Electron Microscopy (TEM) and Histological Analysis

Histological specimens for light microscopy were processed as previously described.[30] In brief, embryos were fixed in primary fixative [2% paraformaldehyde, 2.5% glutaraldehyde, 3% sucrose, 0.06% phosphate buffer (pH 7.4)] at 4°C for 24 h and then washed in 0.1 M PBS, dehydrated through an ethanol series and propylene oxide and then infiltrated with EMbed-812/Araldyte resin mixture. Semi-thin plastic sections were cut with a glass knife on a JB4 microtome and stained with 1% Toluidine blue in 1% Borax. For TEM, an additional fixation in 1.0% Osmium was included, followed by dehydration in MeOH/Aralhydrate. Embryos were then embedded in EMBed-812/DER 736. Ultrathin sections (60–70 nm) were collected on coated grids and stained with uranyl acetate and lead citrate for contrast. Images were captured using Hitachi H600 TEM.

### Frozen Section Immunohistochemistry

Wild-type and morphant embryos were fixed in 4 % paraformaldehyde/PBS and infiltrated with 2-hour steps of 15 % sucrose, 30 % sucrose and 100 % Tissue-Tek OCT. Embryos were orientated, sectioned, and mounted on gelatin-coated glass slides. Antibodies that recognize Laminin -111 (Laminin-1 epitope, Sigma L9393; 1:200 dilution) were used in a 5 % Goat Serum/PBT blocking solution. This antibody was raised against purified basement membranes and affinity purified against entire Laminin-111 heterotrimer. Immunoreactivity was detected with fluorescent a secondary antibody and imaged with a Nikon C1 confocal microscope.

### Microangiography

Fluorescently labeled 2MDa dextrans were injected into the tail vein or sinus venosus of 2–5dpf, PTU treated, anesthetized Tg(*fli1a*:GFP) zebrafish embryos as previously described.[31] Embryos were mounted in 1% low-melt agarose and injections were done using a Drummond Nanoject (Drummond Scientific Co, Broomall, PA) with micropipettes cut to a bore size of 5–10 μM. Distribution of dextrans throughout the vasculature was monitored through a fluorescent dissecting microscope and imaging was done with a Nikon C1 confocal microscope.

## RESULTS

### Zebrafish *foxC1a* and *foxC1b* are expressed in the periocular mesenchyme and developing vasculature

Expression of *foxC1a* and *foxC1b* were assessed during development by *in situ* hybridization. As previously reported, we found both genes expressed in the paraxial mesoderm, head mesenchyme, and vascular system before 24 hours post fertilization (hpf) (data not shown; [22]). By 24 hfp, strong expression of *foxC1a* was found in the periocular

NIH-PA Author Manuscript

NIH-PA Author Manuscript

NIH-PA Author Manuscript

mesenchyme (Figure 1A,C). Levels in the periocular mesenchyme peaked between 24 and 36 hpf, and then gradually decreased over time (Figure 1A,C). In the developing hyaloid vasculature, levels of *foxC1a* expression correlated with expression in the periocular mesenchyme (Figure 1C). Expression of *foxC1a* was also maintained in endothelial cells of the developing trunk vasculature (Figure 1D). From 72–96 hpf, strongest expression of *foxC1a* was found in the branchial arches (Figure 1A,C). *foxC1b* showed both overlapping and distinct patterns and timing of expression as compared to *foxC1a*. In the periocular mesenchyme, expression lagged behind *foxC1a*, with levels not detectable until 36 hpf, but then persisting later during development (Figure 1 B,C). Expression in trunk vascular endothelial cells was evident at all times assessed, though levels in the hyaloid were below detection by whole mount in situ hybridization (Figure 1 B,C,D). Overall, strongest expression of *foxC1b* was in the branchial arch region and the fin buds (Figure 1B,C).

### Loss of *foxC1* results in vascular defects

To address loss of function phenotypes during zebrafish development, morpholinos were used to knock down both *foxC1* genes. The morpholinos used were originally described to assess phenotypes during early somitogenesis (<18 hpf).[27] For both *foxC1a* and *foxC1b*, two independent morpholinos were designed to specifically target each gene. As both genes contain only one exon, morpholinos were designed to target the ATG start codon and 5′ untranslated regions. For both genes, injection of either morpholino resulted in similar phenotypes. The morpholinos targeting the ATG start codons were effective at lower doses and these were used for the remainder of our studies. Phenotypes were unchanged when a morpholino targeting *p53* was co-injected, indicating the morpholinos do not promote phenotypes through off-target mediated cell death.[32] Knock-down of *foxC1a* resulted in a number of gross phenotypes, including hydrocephaly, heart edema, a small eye, and variable hemorrhage within the CNS and eyes (Figure 2A). When *foxC1b* was targeted, no obvious phenotypes were observed except a slight developmental delay which is common with morpholino injections (Figure 2A). Based on gene similarity, we hypothesized the lack of gross phenotypes, may be due to compensation by *foxC1a*. This also raised the possibility that *foxC1b* may compensate to some degree for loss of *foxC1a*. To address this, morpholinos targeting both genes were co-injected and compared to embryos injected with the individual morpholinos plus control morpholino to maintain equal total morpholino concentrations. No additional phenotypes were observed as compared to *foxC1a* morphants, but the severity of phenotypes was increased (Figure 2A). The remaining studies were done with a combination of morpholinos targeting both *foxC1* genes (*foxC1*dMOs).

To explore the hemorrhage phenotypes in more detail, we tested several doses of *foxC1*dMOs and quantified the phenotypes. In our initial studies of *foxC1*dMO, we found that ocular and CNS hemorrhaging phenotypes presented with variable penetrance. Interestingly, the number of embryos with hemorrhages in *foxC1*dMO embryos decreased as compared to embryos injected with *foxC1a* MO alone. The reduction of hemorrhages in *foxC1*dMO morphants correlated with a lack of blood flow which was noted in the majority of these embryos (Figure 2B,C,D). Blood cells were present in *foxC1*dMO embryos, but most often accumulated in the tail veins (Figure 2B). Lowering the dosage of *foxC1*dMO (1.65ng of each morpholino/embryo as compared to 3.25 ng/embryo), restored blood flow in the majority of embryos, but also increased the number of hemorrhages (Figure 2B,D). This result is consistent with the requirement of blood flow in the development of vascular hemorrhaging following loss of *foxC1* function.

As the majority of hemorrhages in *foxC1* morphants were confined to the CNS and eyes, we examined semi-thin histological sections of these regions to evaluate gross vessel morphology. Dilated, hydrocephalic ventricles were apparent in the CNS, but no gross differences in vessels were noted (Figure 3A). As described for other species, the eyes were

NIH-PA Author Manuscript

NIH-PA Author Manuscript

NIH-PA Author Manuscript

small and lacked proper anterior segment development (Figure 3A). Specifically, the cornea was thickened with decreased corneal endothelial cells and poorly condensing corneal stroma (Figure 3A). Cells within the developing iridiocorneal angle, as well as periocular cells overall, appeared loosely organized and undifferentiated (Figure 3A) To further assess the state of periocular cells, which arise from migrating neural crest cells, we examined *foxC1* knockdown in a transgenic zebrafish line which has a subset of neural crest cells labeled with GFP (Tg(*foxd3*:GFP)$^{zf15}$).[48] Analysis through development shows neural crest cells in *foxC1*dMO embryos do migrate around to the anterior eye, but are fewer in number and retain an immature morphology as compared to controls (Figure 3B, Supplemental Figure 1). Assessment of fully formed anterior segment structures was not possible as maturation occurs after 72 hpf, when morpholinos no longer have a primary affect on protein expression. Examination of the retina in *foxC1*dMOs also revealed defects. At 48 hpf, lamination of the neural retina was slightly delayed in *foxC1*dMO embryos and eye size was reduced overall (Figure 3A, B). Striking differences in the morphology of the hyaloid vessels were also noted. In control eyes, multiple, small vessels were found between the lens and the retina (Figure 3A, right panels). In contrast, one or two large, dilated vessels were observed in *foxC1*dMO morphant eyes at the same position between the lens and retina (Figure 3A and Figure 6A–C). In addition, there were often undifferentiated cells behind the lens in *foxC1*dMO morphant eyes (Figure 6E). A slight delay in lens development was also noted, but cellular morphology judged by semi-thin histology and TEM did not reveal defects (Figure 3A, Figure 6A–E).

### Vascular endothelial fate and morphology are disrupted in *foxC1* morphant embryos

To further investigate the vascular phenotypes in *foxC1* morphants, knockdown experiments were done in the vascular endothelial reporter transgenic line, Tg(*fli1a*:EGFP)$^{y5}$. This transgenic line allows visualization of the entire vasculature throughout development.[33] A number of interesting phenotypes were observed with injection of the high morpholino dose described above. Confocal imaging of the dorsal aorta and cardinal vein revealed inappropriate luminal connections throughout the tail, suggestive of arterial-venous cell fate defects (Figure 4A). Consistent with this interpretation, the venous marker *flt4* showed ectopic expression in vessels of the dorsal aorta (Figure 4B). Analysis of vessels in the anterior embryo also showed disruption. In this region, the paired lateral dorsal aortae normally join to form the single midline dorsal aorta (Figure 4A). Embryos depleted of *foxC1* showed thin and disorganized vessels in this region (Figure 4A). The use of the Tg(*fli1a*:GFP) line also helped resolve defects in the hyaloid vasculature. By 48 hpf in control embryos, an organized vascular basket envelops the lens (Figure 4A; [34]). In some *foxC1*dMO morphants, *fli1a*:GFP positive cells were present, but collected in an undifferentiated mass behind the lens (Figure 4A). However, in other morphant embryos, hyaloid vessel differentiation did occur, but as suggested by histology, resulted in a less branched and dilated morphology (Figure 4C). Expression of *flt4* in the hyaloid was similar in *foxC1*dMO morphants as compared to control embryos (Figure 4B), indicating that the cellular defects were not due to altered endothelial cell fate determination and instead due to disrupted differentiation.

To assess blood flow and vasculature integrity in *foxC1*dMO morphants, microangiography with tetramethyl-rhodamine labeled 2MDa dextrans was performed in Tg(*fli1a*:GFP) embryos. Injection of dextrans into tail veins of *foxC1*dMOs showed a decreased capacity to flow throughout the vasculature as compared to controls. Injections often resulted in ruptured trunk vessels and dye accumulation into the yolk (Figure 4C). When flow of dextrans was achieved to the head, accumulation in hydrocephalic brain ventricles was observed, indicating compromised vessel integrity (Figure 4C). Within the eye,

NIH-PA Author Manuscript

NIH-PA Author Manuscript

NIH-PA Author Manuscript

accumulation of dye was observed behind the lens, but was typically confined by *fli1a*:GFP positive cells when vessel formation occurred (Figure 4C).

Because hemodynamic forces have been shown to regulate endothelial cell differentiation, we analyzed vessel formation in lower dose *foxC1*dMO, Tg(*fli1a*:GFP) embryos where blood flow was normal. In these embryos overt vascular morphology appeared normal in trunk regions and within the eye (Figure 5A). Confocal microscopy, however, revealed disorganization of endothelial cells and excess branching of trunk intersegmental vessels at 24hpf (Figure 5B). Injection of labeled 2MDa dextrans into low-dose morphant embryos at 48 and 72 hpf did not show increased overall permeability. However, by 96 hpf *foxC1*dMO embryos did show increased dextran permeability within the CNS and eye (Figure 5C).

## Loss of *foxC1* results in vascular basement membrane defects

To explore the observed vascular phenotypes in more depth, hyaloid vessels from high dose *foxC1*dMO embryos were analyzed by TEM. In *foxC1*dMO embryos endothelial cells were dilated, but showed normal morphology and cell-cell junctions as compared to controls (Figure 6). As predicted by histology, undifferentiated mesenchymal cells were also often found behind the lens of *foxC1*dMO embryos (Figure 6E). In addition to mesenchymal cell differentiation and vessel morphology defects in *foxC1*dMO eyes, TEM revealed disruptions to basement membrane present between hyaloid vessels and both the lens and the retina (Figure 6B). In controls, a smooth, continuous basement membrane was present along the entire basal surface of the lens and retina (Figure 6F,H, J, L). In *foxC1*dMOs, the basement membrane was disorganized and showed focal disruptions (Figure 6G, I, K, M).

To confirm the basement membrane disruptions in *foxC1*dMOs, immunostaining for Laminin-111 was performed. Laminins, along with type IV collagens, Nidogen and sulfated proteoglycans make up the normal components of all basement membranes. Laminin-111 is a heterotrimeric glycoprotein composed of one alpha, one beta and one gamma chain. In control embryos, a smooth, uninterrupted staining pattern was observed along both the basal surface of the retina and along the lens (Figure 7). In contrast, Laminin-111 staining was more diffuse with interruptions along the lens and retinal surfaces in *foxC1*dMO eyes (Figure 7).

## *foxc1* and *laminin alpha-1* show genetic interaction

Many of the vascular defects in *foxC1*dMO embryos are reminiscent of vascular anomalies caused by loss of *laminin alpha-1*(*lama1*) function. The *lama1* gene encodes for the alpha subunit of the Laminin-111 complex. To investigate the relationship between *foxc1* and the basement membrane component *lama1,* zebrafish embryos were co-injected with morpholinos targeting the *foxC1* genes and *lama1. lama1* has been previously investigated in the zebrafish, and homozygous mutations in this gene (*bashful*) or morpholino knockdown result in lens degeneration, hyaloid and trunk vasculature defects, and body truncations.[28, 29, 35] When previously described concentrations of this morpholino were co-injected with either the high or low doses of *foxc1* morpholinos described above, severe body truncation phenotypes were observed (data not shown). To further investigate the combined effects of *foxc1* and *lama1* knockdown, sub-maximal doses of all morpholinos were injected. Very mild hydrocephalic and hemorrhaging phenotypes were observed when 1.3ng of each *foxC1* morpholino were injected alone (Figure 8A,B). When 3.9 ng of *lama1* morpholino was co-injected with these concentrations of *foxC1*dMO, the incidence and severity of both hemorrhaging and hydrocephaly were increased (Figure 8A,B). This concentration of *lama1* morpholino injected alone showed only occasional, mild lens and tail defects, along with a small number embryos with mild hydrocephaly and hemorrhage (Figure 8A,B). Finally, we also studied knockdown of *foxC1* in homozygous *bashful/lama1*

NIH-PA Author Manuscript

NIH-PA Author Manuscript

NIH-PA Author Manuscript

mutants (*bal*$^{b69}$). Injection of sub-maximal *foxC1*dMO into these embryos resulted in more severe phenotypes than mutants alone, including increased severity of the tail and lens phenotypes and a more pronounced hydrocephaly (data not shown). We also tested *foxC1* knockdown in embryos heterozygous for the *bal*$^{b69}$ mutation, but did not observe any differences as compared to the wild-type siblings.

## DISCUSSION

In this study we describe the effects of *foxC1* knockdown on zebrafish larvae. We found that the overall spectrum of phenotypes due to loss of *foxC1* in the zebrafish is similar to those found with loss of *FOXC1* in mammals, indicating a conservation of function across species. We focused our investigation on how loss of *foxC1* impacts ocular and CNS vascular development. Knock-down of *foxC1* resulted in defects in vascular endothelial cell fate and differentiation and disrupted vessel morphology and integrity. Interestingly, we found that loss of *foxC1* leads to disruption of vascular basement membrane structure and *foxC1* genetically interacts with *lama1*, which encodes a key component of the basement membrane.

In mouse, combined deletion of *Foxc1* and *Foxc2* result in severe vascular phenotypes including defects in arterial-venous fate decisions and concomitant arterial-venous malformations, as well as aorta coarctation.[16, 18, 19] Arterial versus venous specification occurs by differential VEGF activity and subsequent reciprocal Eph/Ephrin signaling (reviewed in [36]). EphrinB2 expression in arterial cells occurs by activation of the Notch pathway and Hey2 activation. FOXC1 and FOXC2 have been implicated in multiple steps in this pathway, and both have been shown to directly activate Notch target genes in response to VEGF signaling.[19, 20] In our studies, we found similar arterial-venous defects in severe loss of *foxC1*dMO embryos. In addition to expansion of the venous marker *flt4,* arterial-venous malformations were reveled by *fli1a:*GFP. The vessel defects in the tails and the aorta coarctation of *foxC1*dMO embryos are similar to those described for zebrafish *gridlock* mutants, in which Hey2 function is disrupted.[31] Defects in the trunk vessels and aorta help explain the lack of proper blood flow found in severe *foxC1*dMO embryos.

While *foxC1* is important for arterial specification in the trunk vessels, it is unclear if this also accounts for the severe phenotypes observed in the hyaloid vasculature. In mammals, the hyaloid is an entirely arterial system and is devoid of veins.[37] This led to an initial hypothesis that defects in arterial specification may cause the hyaloid defects in *foxC1*dMO embryos. However, in zebrafish the venous marker *flt4* was expressed in both wild-type and *foxC1*dMO hyaloid vessels, indicating differences exist in the zebrafish hyaloid as compared to mammals. This may be indicative of the different fates these vascular beds have in the zebrafish versus mammals. The hyaloid system is a transient structure in mammals, and its regression is required for proper retinal vessel development (reviewed in [37]). In contrast, the zebrafish hyaloid system does not regress, but instead migrates and grows with the retina to form the mature vitreal-retinal vascular system.[34]

While endothelial cell fate defects cannot explain the hyaloid defects in *foxC1* morphants, clues were provided by additional experiments. Fluorescent dextrans injected into the vasculature of *foxC1*dMOs showed that vessel integrity was compromised and permeability was increased. We hypothesized this may be due to defects in endothelial cell-cell junction formation. Indeed, junctional complexes are disrupted in the cornea of *Foxc1* knock-out mice.[12] However, TEM analysis of vessels in *foxC1*dMOs showed morphologically normal inter-endothelial cell junctions.

NIH-PA Author Manuscript

NIH-PA Author Manuscript

NIH-PA Author Manuscript

Ultrastructural analyses did reveal disruptions in the basement membranes between hyaloid vessels and the lens and retina. Staining for Laminin-111 in *foxC1*dMO embryos confirmed basement membrane defects. As *lama1* mutants show defects in the development of the hyaloid and trunk vascular system similar to those of *foxC1* morphants [28, 35], we also explored the genetic interaction between *foxC1* and *lama1* genes. Combined sub-maximal knock-down of *foxC1* and *lama1* genes resulted in vascular phenotypes similar to those observed in full-dose, severe *foxC1*dMO embryos. These data suggest that FoxC1 regulates factor(s) essential for normal basement membrane formation or maintenance.

We posit that basement membrane defects result in the increased permeability and hemorrhaging in CNS vessels that were observed upon tracer dye injection. Basement membrane defects may also disrupt proper differentiation of vascular cells in the hyaloid, leading to the dilated vessel morphology and accumulation of undifferentiated periocular mesenchymal cells behind the lens in *foxC1* morphants. The delay in retinal lamination found in *foxC1*dMO eyes may also be explained by the lack of a mature basement membrane on the basal surface of the retina. This is supported by the recent finding that focal disruptions in meningeal basement membrane result in lamination defects in the cortex of the mouse *Foxc1* hypomorph.[14] Additionally, zebrafish mutant for either *pak2a* or *beta-pix* result in hydrocephalus and CNS hemorrhaging, similar to *foxC1*dMO embryos.[38, 39] *pak2a* and *beta-pix* function together downstream of integrin signaling and were shown to be required for proper maintenance of the basement membrane surrounding CNS vessels.[38, 39] Cumulatively, these findings suggest that defects in production or maintenance of basement membrane components may underlie aspects of vascular defects found with loss of *foxC1.*

The disruption of basement membrane integrity in *foxC1* morphants provides insight into *FOXC1* disease phenotypes. Vascular basement membrane defects have implications for the development of glaucoma in *FOXC1* patients. Integrity of retinal vessels is important to maintain the blood retinal barrier and defects affecting vascular permeability are known to impact glaucoma (reviewed in [40]). Vascular tone and permeability are also under the influence of systemic factors, both environmental and genetic, and this may represent a focal point where *FOXC1* disease can be modified. Finally, mutations in the basement membrane constituent Collage IV alpha 1 (*COL4A1*), correlate with increased incidence of stroke and are associated with Axenfeld-Reiger anomaly in humans.[41–45] Indeed, one recognized cause of stroke is the localized breakdown of vessel integrity and *Col4a1* knockout mice show hemorrhagic stroke and ASD phenotypes.[43, 46, 47] Increased mortality in *FOXC1* patients nor potential relationships between *FOXC1* mutations and vascular compromise have not been reported, but, together, this data suggests that *FOXC1* patients may have an increased risk for stroke.

## Acknowledgments

We thank Michael Cliff for technical assistance and animal husbandry, and Clive Wells for assistance with TEM. We also gratefully acknowledge the following funding support: T32EYE014537, Research training program in vision sciences (JMS), F30AG029763 (JMS), NIH R01EY16060 (BAL), and NEI Core Facilities grant P30EY001931 to the vision research community of MCW.

## References

1. Nishimura DY, Swiderski RE, Alward WL, et al. The forkhead transcription factor gene FKHL7 is responsible for glaucoma phenotypes which map to 6p25. Nat Genet. 1998; 19:140–147. [PubMed: 9620769]
2. Kume T, Deng KY, Winfrey V, Gould DB, Walter MA, Hogan BL. The forkhead/winged helix gene Mf1 is disrupted in the pleiotropic mouse mutation congenital hydrocephalus. Cell. 1998; 93:985–996. [PubMed: 9635428]

NIH-PA Author Manuscript

NIH-PA Author Manuscript

NIH-PA Author Manuscript


3. Lehmann OJ, Ebenezer ND, Jordan T, et al. Chromosomal duplication involving the forkhead transcription factor gene FOXC1 causes iris hypoplasia and glaucoma. Am J Hum Genet. 2000; 67:1129–1135. [PubMed: 11007653]
4. Mears AJ, Mirzayans F, Gould DB, Pearce WG, Walter MA. Autosomal dominant iridogoniodysgenesis anomaly maps to 6p25. Am J Hum Genet. 1996; 59:1321–1327. [PubMed: 8940278]
5. Nishimura DY, Searby CC, Alward WL, et al. A spectrum of FOXC1 mutations suggests gene dosage as a mechanism for developmental defects of the anterior chamber of the eye. Am J Hum Genet. 2001; 68:364–372. [PubMed: 11170889]
6. Saleem RA, Banerjee-Basu S, Berry FB, Baxevanis AD, Walter MA. Analyses of the effects that disease-causing missense mutations have on the structure and function of the winged-helix protein FOXC1. Am J Hum Genet. 2001; 68:627–641. [PubMed: 11179011]
7. Saleem RA, Banerjee-Basu S, Berry FB, Baxevanis AD, Walter MA. Structural and functional analyses of disease-causing missense mutations in the forkhead domain of FOXC1. Hum Mol Genet. 2003; 12:2993–3005. [PubMed: 14506133]
8. Saleem RA, Murphy TC, Liebmann JM, Walter MA. Identification and analysis of a novel mutation in the FOXC1 forkhead domain. Invest Ophthalmol Vis Sci. 2003; 44:4608–4612. [PubMed: 14578375]
9. Shields MB, Buckley E, Klintworth GK, Thresher R. Axenfeld-Rieger syndrome. A spectrum of developmental disorders. Surv Ophthalmol. 1985; 29:387–409. [PubMed: 3892740]
10. Strungaru MH, Dinu I, Walter MA. Genotype-phenotype correlations in Axenfeld-Rieger malformation and glaucoma patients with FOXC1 and PITX2 mutations. Invest Ophthalmol Vis Sci. 2007; 48:228–237. [PubMed: 17197537]
11. Walter MA, Mirzayans F, Mears AJ, Hickey K, Pearce WG. Autosomal-dominant iridogoniodysgenesis and Axenfeld-Rieger syndrome are genetically distinct. Ophthalmology. 1996; 103:1907–1915. [PubMed: 8942889]
12. Kidson SH, Kume T, Deng K, Winfrey V, Hogan BL. The forkhead/winged-helix gene, Mf1, is necessary for the normal development of the cornea and formation of the anterior chamber in the mouse eye. Dev Biol. 1999; 211:306–322. [PubMed: 10395790]
13. Gruneberg H. Congenital hydrocephalus in the mouse, a case of spurious pleitropism. J Genet. 1943; 45:1–21.
14. Zarbalis K, Siegenthaler JA, Choe Y, May SR, Peterson AS, Pleasure SJ. Cortical dysplasia and skull defects in mice with a Foxc1 allele reveal the role of meningeal differentiation in regulating cortical development. Proc Natl Acad Sci U S A. 2007; 104:14002–14007. [PubMed: 17715063]
15. Smith RS, Zabaleta A, Kume T, et al. Haploinsufficiency of the transcription factors FOXC1 and FOXC2 results in aberrant ocular development. Hum Mol Genet. 2000; 9:1021–1032. [PubMed: 10767326]
16. Kume T, Deng K, Hogan BL. Murine forkhead/winged helix genes Foxc1 (Mf1) and Foxc2 (Mfh1) are required for the early organogenesis of the kidney and urinary tract. Development. 2000; 127:1387–1395. [PubMed: 10704385]
17. Kume T, Jiang H, Topczewska JM, Hogan BL. The murine winged helix transcription factors, Foxc1 and Foxc2, are both required for cardiovascular development and somitogenesis. Genes Dev. 2001; 15:2470–2482. [PubMed: 11562355]
18. Winnier GE, Kume T, Deng K, et al. Roles for the winged helix transcription factors MF1 and MFH1 in cardiovascular development revealed by nonallelic noncomplementation of null alleles. Dev Biol. 1999; 213:418–431. [PubMed: 10479458]
19. Seo S, Fujita H, Nakano A, Kang M, Duarte A, Kume T. The forkhead transcription factors, Foxc1 and Foxc2, are required for arterial specification and lymphatic sprouting during vascular development. Dev Biol. 2006; 294:458–470. [PubMed: 16678147]
20. Hayashi H, Kume T. Foxc transcription factors directly regulate Dll4 and Hey2 expression by interacting with the VEGF-Notch signaling pathways in endothelial cells. PLoS ONE. 2008; 3:e2401. [PubMed: 18545664]

NIH-PA Author Manuscript

NIH-PA Author Manuscript

NIH-PA Author Manuscript


21. Hayashi H, Kume T. Forkhead transcription factors regulate expression of the chemokine receptor CXCR4 in endothelial cells and CXCL12-induced cell migration. Biochem Biophys Res Commun. 2008; 367:584–589. [PubMed: 18187037]
22. Topczewska JM, Topczewski J, Solnica-Krezel L, Hogan BL. Sequence and expression of zebrafish foxc1a and foxc1b, encoding conserved forkhead/winged helix transcription factors. Mech Dev. 2001; 100:343–347. [PubMed: 11165495]
23. McMahon C, Semina EV, Link BA. Using zebrafish to study the complex genetics of glaucoma. Comp Biochem Physiol C Toxicol Pharmacol. 2004; 138:343–350. [PubMed: 15533792]
24. Thompson MA, Ransom DG, Pratt SJ, et al. The cloche and spadetail genes differentially affect hematopoiesis and vasculogenesis. Dev Biol. 1998; 197:248–269. [PubMed: 9630750]
25. Thisse B, Heyer V, Lux A, et al. Spatial and temporal expression of the zebrafish genome by large-scale in situ hybridization screening. Methods Cell Biol. 2004; 77:505–519. [PubMed: 15602929]
26. Thisse C, Thisse B. High-resolution in situ hybridization to whole-mount zebrafish embryos. Nat Protoc. 2008; 3:59–69. [PubMed: 18193022]
27. Topczewska JM, Topczewski J, Shostak A, Kume T, Solnica-Krezel L, Hogan BL. The winged helix transcription factor Foxc1a is essential for somitogenesis in zebrafish. Genes Dev. 2001; 15:2483–2493. [PubMed: 11562356]
28. Semina EV, Bosenko DV, Zinkevich NC, et al. Mutations in laminin alpha 1 result in complex, lens-independent ocular phenotypes in zebrafish. Dev Biol. 2006; 299:63–77. [PubMed: 16973147]
29. Zinkevich NS, Bosenko DV, Link BA, Semina EV. laminin alpha 1 gene is essential for normal lens development in zebrafish. BMC Dev Biol. 2006; 6:13. [PubMed: 16522196]
30. Soules KA, Link BA. Morphogenesis of the anterior segment in the zebrafish eye. BMC Dev Biol. 2005; 5:12. [PubMed: 15985175]
31. Weinstein BM, Stemple DL, Driever W, Fishman MC. Gridlock, a localized heritable vascular patterning defect in the zebrafish. Nat Med. 1995; 1:1143–1147. [PubMed: 7584985]
32. Robu ME, Larson JD, Nasevicius A, et al. p53 activation by knockdown technologies. PLoS Genet. 2007; 3:e78. [PubMed: 17530925]
33. Lawson ND, Weinstein BM. In vivo imaging of embryonic vascular development using transgenic zebrafish. Dev Biol. 2002; 248:307–318. [PubMed: 12167406]
34. Alvarez Y, Cederlund ML, Cottell DC, et al. Genetic determinants of hyaloid and retinal vasculature in zebrafish. BMC Dev Biol. 2007; 7:114. [PubMed: 17937808]
35. Pollard SM, Parsons MJ, Kamei M, et al. Essential and overlapping roles for laminin alpha chains in notochord and blood vessel formation. Dev Biol. 2006; 289:64–76. [PubMed: 16321372]
36. Lamont RE, Childs S. MAPping out arteries and veins. Sci STKE. 2006; 2006:pe39. [PubMed: 17018851]
37. Saint-Geniez M, D'Amore PA. Development and pathology of the hyaloid, choroidal and retinal vasculature. Int J Dev Biol. 2004; 48:1045–1058. [PubMed: 15558494]
38. Buchner DA, Su F, Yamaoka JS, et al. pak2a mutations cause cerebral hemorrhage in redhead zebrafish. Proc Natl Acad Sci U S A. 2007; 104:13996–14001. [PubMed: 17715297]
39. Liu J, Fraser SD, Faloon PW, et al. A betaPix Pak2a signaling pathway regulates cerebral vascular stability in zebrafish. Proc Natl Acad Sci U S A. 2007; 104:13990–13995. [PubMed: 17573532]
40. Flammer J, Mozaffarieh M. What is the present pathogenetic concept of glaucomatous optic neuropathy? Surv Ophthalmol. 2007; 52 (Suppl 2):S162–173. [PubMed: 17998042]
41. Gould DB, Phalan FC, van Mil SE, et al. Role of COL4A1 in small-vessel disease and hemorrhagic stroke. N Engl J Med. 2006; 354:1489–1496. [PubMed: 16598045]
42. Plaisier E, Gribouval O, Alamowitch S, et al. COL4A1 mutations and hereditary angiopathy, nephropathy, aneurysms, and muscle cramps. N Engl J Med. 2007; 357:2687–2695. [PubMed: 18160688]
43. Sibon I, Coupry I, Menegon P, et al. COL4A1 mutation in Axenfeld-Rieger anomaly with leukoencephalopathy and stroke. Ann Neurol. 2007; 62:177–184. [PubMed: 17696175]

NIH-PA Author Manuscript

NIH-PA Author Manuscript

NIH-PA Author Manuscript

44. Vahedi K, Boukobza M, Massin P, Gould DB, Tournier-Lasserve E, Bousser MG. Clinical and brain MRI follow-up study of a family with COL4A1 mutation. Neurology. 2007; 69:1564–1568. [PubMed: 17938367]

45. Vahedi K, Kubis N, Boukobza M, et al. COL4A1 mutation in a patient with sporadic, recurrent intracerebral hemorrhage. Stroke. 2007; 38:1461–1464. [PubMed: 17379824]

46. Favor J, Gloeckner CJ, Janik D, et al. Type IV procollagen missense mutations associated with defects of the eye, vascular stability, the brain, kidney function and embryonic or postnatal viability in the mouse, Mus musculus: an extension of the Col4a1 allelic series and the identification of the first two Col4a2 mutant alleles. Genetics. 2007; 175:725–736. [PubMed: 17179069]

47. Gould DB, Phalan FC, Breedveld GJ, et al. Mutations in Col4a1 cause perinatal cerebral hemorrhage and porencephaly. Science. 2005; 308:1167–1171. [PubMed: 15905400]

48. Gilmour DT, Maischein HM, Nüsslein-Volhard C. Migration and function of a glial subtype in the vertebrate peripheral nervous system. Neuron. 2002; 34:577–588. [PubMed: 12062041]

NIH-PA Author Manuscript
NIH-PA Author Manuscript
NIH-PA Author Manuscript



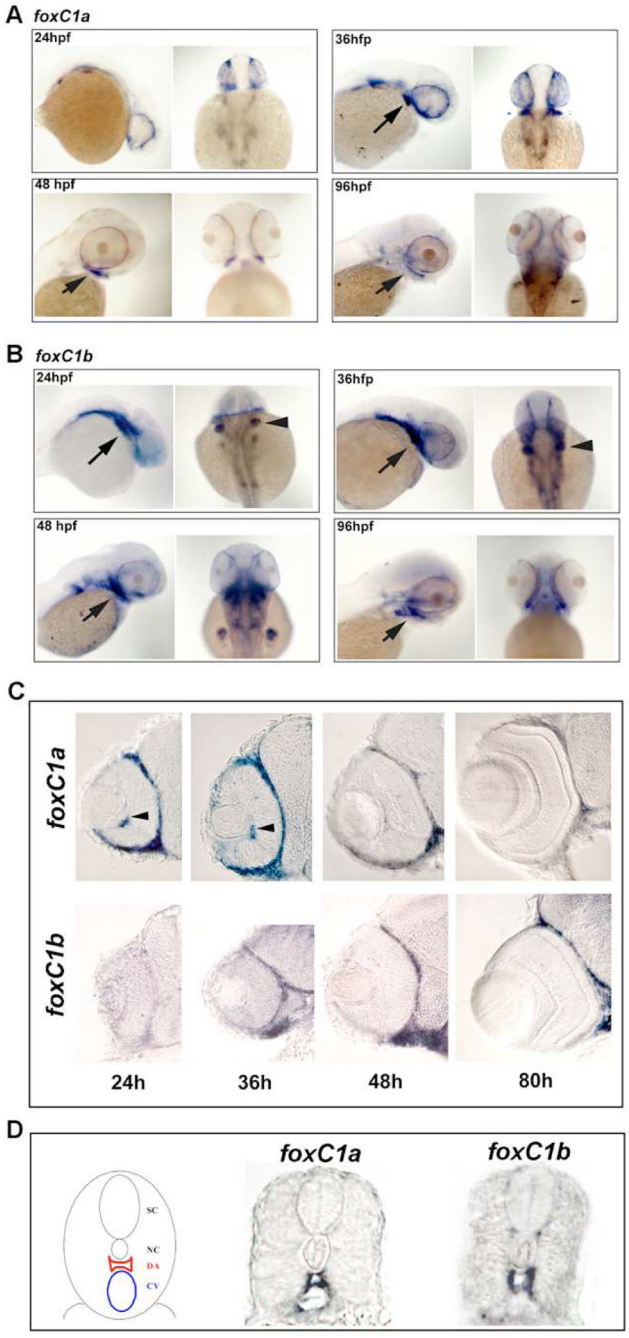


**Figure 1. Expression of *foxC1a* and *foxC1b***

**A.** Whole mount expression of *foxC1a* during development. Strong expression was found in the periocular mesenchyme surrounding the eye at 24–36 hpf. Expression was observed in the branchial arch region (arrows) and in the periocular mesenchyme at 36, 48 and 96hpf. **B.** Whole mount expression of *foxC1b* during development. High levels were found in the branchial arches (arrows) throughout development and in the fin buds (arrow heads) at 24–48 hpf. Periocular mesenchyme expression was absent at 24 hpf, but increased thereafter. **C.** Sections through the eyes showed dynamic expression in the periocular mesenchyme for both *foxC1a* and *foxC1b*. Expression of *foxC1a* was also found in the hyaloid vasculature

(arrows). **D.** Schematic of the zebrafish trunk vasculature (left) and expression of *foxC1a* and *foxC1b* in vascular endothelial cells of the dorsal aorta and the cardinal vein at 36 hpf. SC = Spinal cord, NC = Notocord, DA = Dorsal aorta, CV = Cardinal vein.

NIH-PA Author Manuscript
NIH-PA Author Manuscript
NIH-PA Author Manuscript

NIH-PA Author Manuscript
NIH-PA Author Manuscript
NIH-PA Author Manuscript



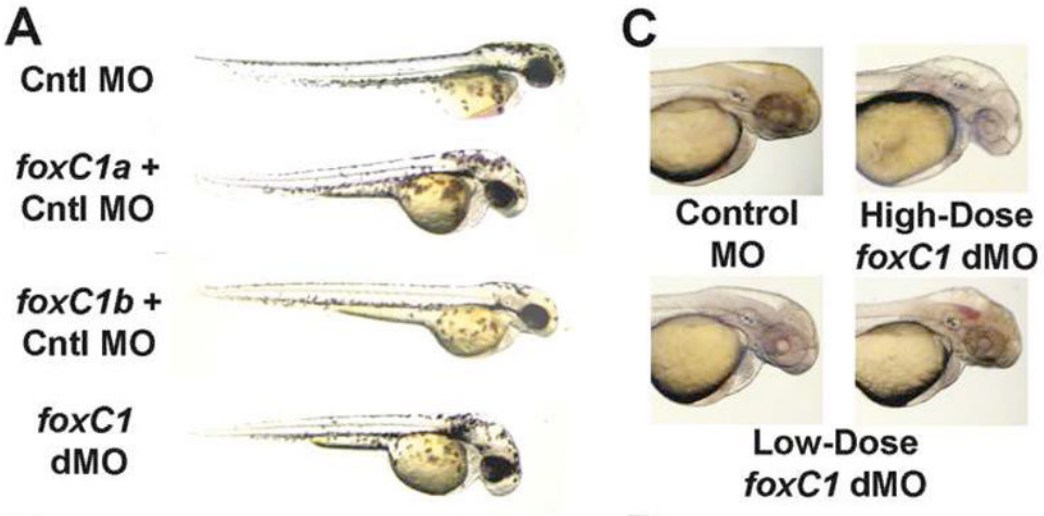


B

| 24 hpf | WT | St. Dev. | foxC1 dMO | St. Dev. | p value |
|---|---|---|---|---|---|
| Heart Rate (bpm) | 70 | 4.42 | 60 | 8.49 | 0.0073 |
| Blood Flow | 45/45 | | 0/37 | | |
| Hemorrhages | 0/45 | | 0/45 | | |

| 48 hpf | WT | St. Dev. | foxC1 dMO | St. Dev. | p value |
|---|---|---|---|---|---|
| Heart Rate (bpm) | 145 | 6.33 | 116 | 15 | 0.0002 |
| Blood Flow | 41/41 | | 6/35 | | |
| Hemorrhages | 0/41 | | 4/35 | | |
| Hemorrhages in Embryos w/ Blood Flow | 0/41 | | 4/6 | | |

| 72 hpf | WT | St. Dev. | foxC1 dMO | St. Dev. | p value |
|---|---|---|---|---|---|
| Heart Rate (bpm) | 137 | 9.67 | 116 | 15 | 0.0005 |
| Blood Flow | 41/41 | | 10/35 | | |
| Hemorrhages | 0/41 | | 7/35 | | |
| Hemorrhages in Embryos w/ Blood Flow | 0/41 | | 7/10 | | |
| Cardiac Edema | 0/41 | | 35/35 | | |
| Hydrocephaly | 0/41 | | 31/35 | | |

D

| Wild Type: | |
|---|---|
| Blood Flow | 27/27 |
| Total w/Hemorrhages | 0 |

| Low dose *foxC1* dMO: | |
|---|---|
| Blood Flow | 24/27 |
| Total w/Hemorrhages | 17/27 |
| Blood Flow + Hemorrhages | 15/24 |

| High dose *foxC1* dMO: | |
|---|---|
| Blood Flow | 6/21 |
| Total w/Hemorrhages | 6/15 |
| Blood Flow + Hemorrhages | 6/6 |

**Figure 2. Gross Phenotypes of *foxC1* Morphants**

**A.** Comparison of Control (Cntl) MO, *foxC1a* + Cntl MO, *foxC1b* + Cntl MO and *foxCa+b* double morphants (*foxC1*dMO) at 48 hpf. Hydrocephaly, heart edema and a small eyes were found in *foxC1a* morphants. Only a slight delay was found with injection of *foxC1b* morpholino. Severity of phenotypes found in *foxC1a* morphants increased in *foxC1*dMO. **B.** Quantification of phenotypes after injection of high dose *foxC1* morpholinos. Heart rates represent an average of 5 embryos, rounded to the nearest integer. Blood flow indicates that blood cells were directly observed flowing throughout the vasculature of the embryo **C.** Dosage-dependent phenotypes of *foxC1*dMO in 48 hpf PTU treated embryos: one control morphant (upper, left), one high-dosage *foxC1*dMO embryo (3.25 ng of each morpholino) (upper, right), and two lower-dose *foxC1*dMO embryos (1.63ng of each morpholino) At high doses, blood flow and hemorrhaging were only occasionally observed. At lower doses, both blood flow and CNS or ocular hemorrhaging was found in the majority of embryos (arrowheads). **D.** Quantification of observed phenotypes with changing dosages of *foxC1* morpholino.

NIH-PA Author Manuscript
NIH-PA Author Manuscript
NIH-PA Author Manuscript



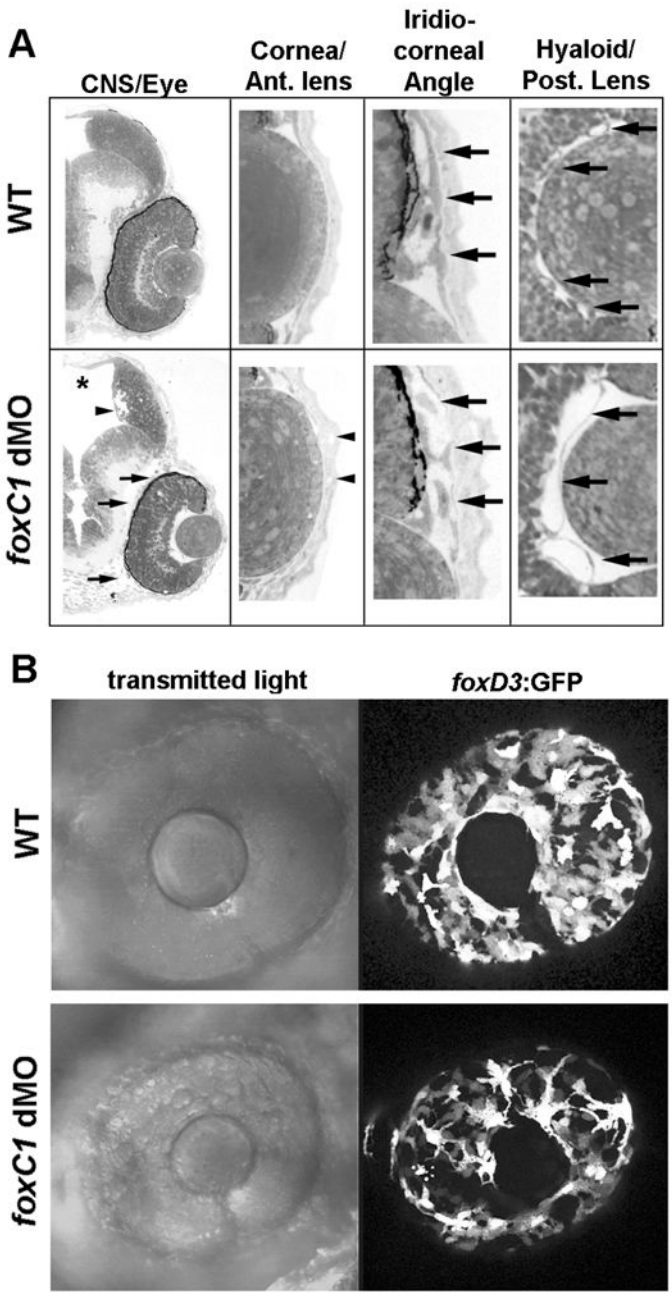


**Figure 3. Assessment of Ocular and CNS development in *foxC1* dMO**

**A.** Histological Examination of 48hpf WT and *foxC1* dMO. Sagittal sections of the brain and eye show expanded ventricles of the brain (askerisk) and the loosely organized periocular mesenchyme (arrows) in *foxC1* dMOs. Areas of cell loss are also noted along the ventricles within the brain (arrow head). High magnification of the cornea and anterior lens shows the corneal endothelium is absent and defects in corneal stroma (arrow heads) are found in *foxC1* dMOs. High magnification of the iridio-corneal angle shows undifferentiated and poorly organized periocular cells (arrows) in *foxC1* dMOs. High magnification of the posteror lens and hyaloid vasculature shows fewer, dilated hyaloid vessels behind the lens (arrows) in *foxC1* dMOs. **B.** Analysis of *foxD3* positive neural crest cells in 48 hpf *foxC1* dMOs. Fewer *foxD3*:GFP positive cells were found migrating to the

anterior of the eye. Cells that have migrated show abnormal morphology as compared to controls.

NIH-PA Author Manuscript

NIH-PA Author Manuscript

NIH-PA Author Manuscript

NIH-PA Author Manuscript
NIH-PA Author Manuscript
NIH-PA Author Manuscript



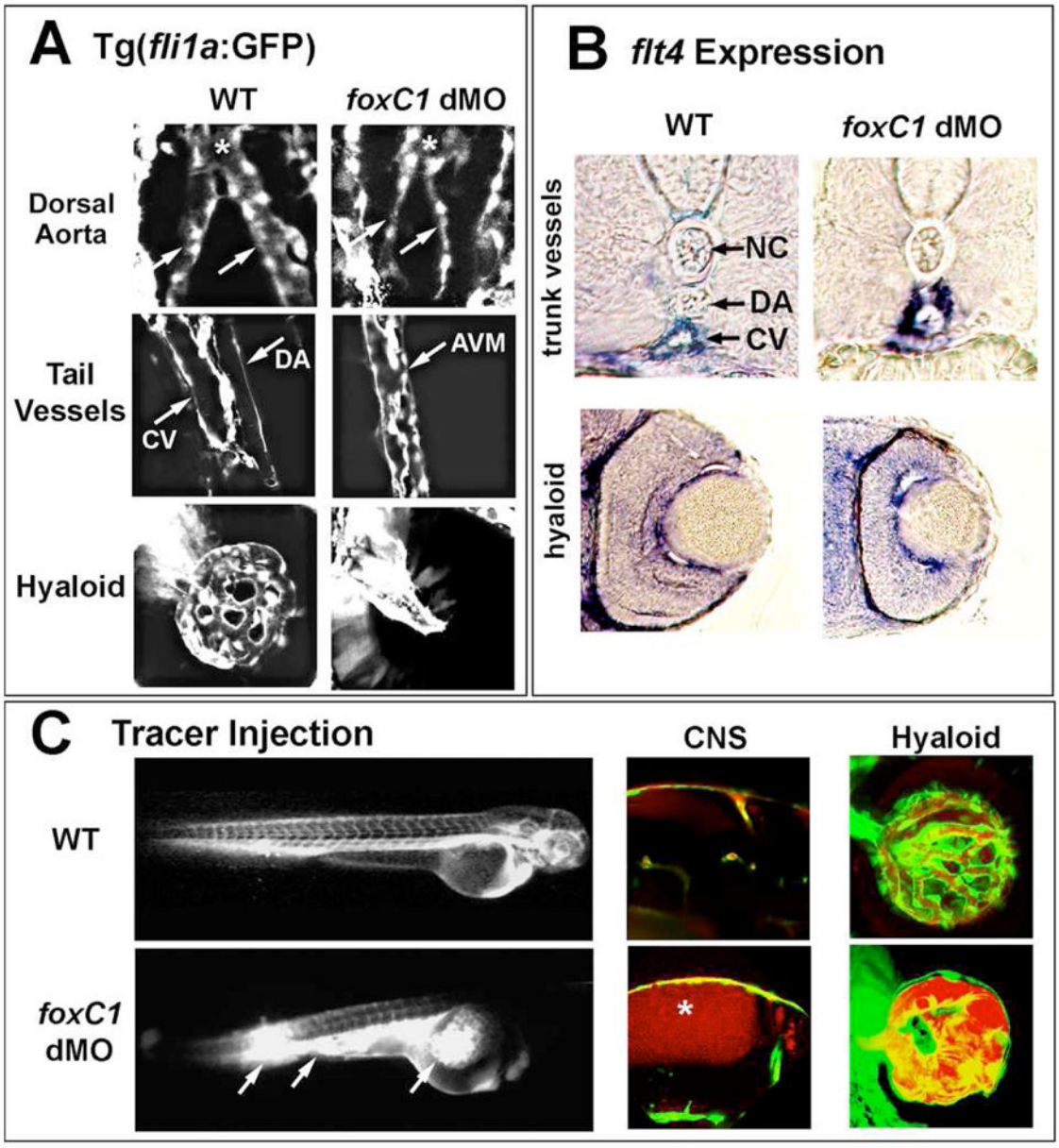


**Figure 4. Vascular phenotypes in high-dose *foxC1*dMO embryos**

**A.** Knockdown of *foxC1* in 48hpf Tg(*fli1a*:GFP) embryos. Defects in dorsal aorta development, axial vessel development and hyaloid vasculature were found in *foxC1* dMOs. Dorsal aortae vessels (arrows) are dysmorphic preceding their fusion (asterisk). In the trunk region, arterial-venous malformations (AVM) are found between the cardinal vein (CV) and the dorsal aorta (DA) in *foxC1*dMOs. Vascular endothelial cells are present in the hyaloid of *foxC1*dMOs, but are less organized than wild-type vessels. **B.** Expression of the venous marker *flt4* was found expanded into the region of the dorsal aorta in *foxC1*dMO embryos (upper panels). See Figure 1D for schematic of anatomy. No differences were observed in *flt4* expression between *foxC1*dMOs and WT within the hyaloid vasculature (lower panels). **C.** Microangiography in *foxC1*dMO, Tg(*fli1a*:GFP) embryos revealed defects in vessel integrity, as shown by breakage of vessels and leakage of dye into the yolk (left panels, arrows). Increased permeability in CNS vessels as revealed by microangiography (center

panels, asterisk). Dye also flowed behind the eye, but was encased by *fli1a*:GFP positive cells (right panels).

NIH-PA Author Manuscript
NIH-PA Author Manuscript
NIH-PA Author Manuscript

NIH-PA Author Manuscript

NIH-PA Author Manuscript

NIH-PA Author Manuscript

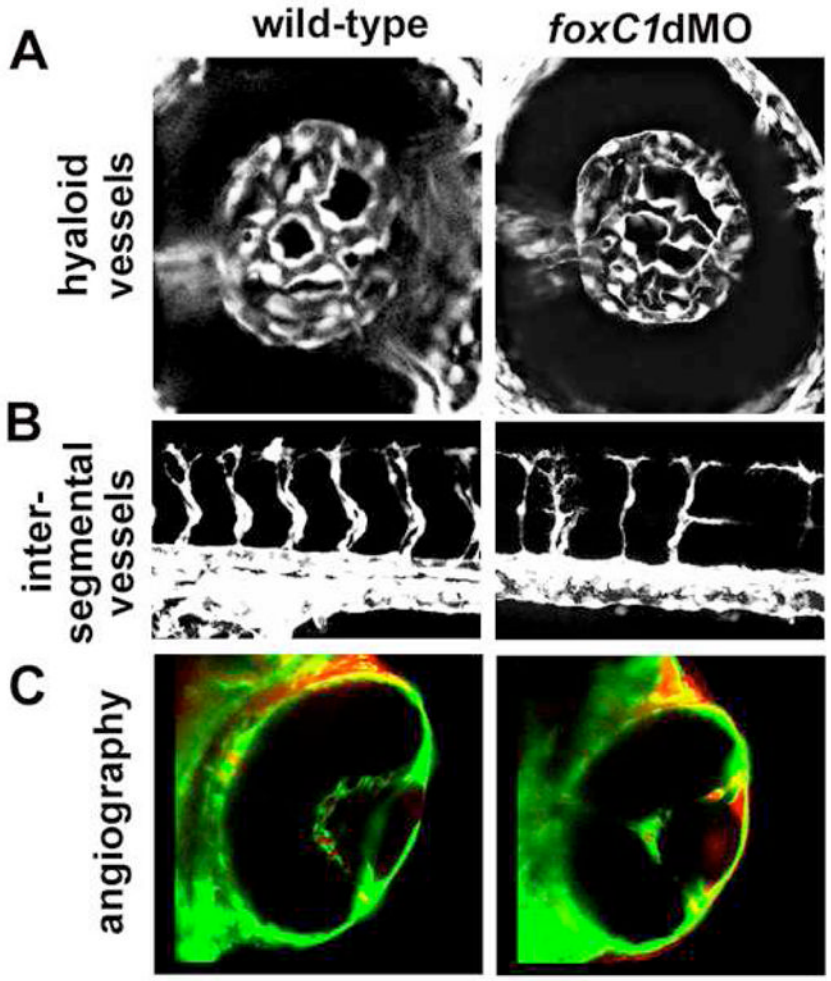


**Figure 5. Vascular phenotypes in low-dose *foxC1*dMO embryos**

**A.** Hyaloid vasculature as revealed by *fli1a*:GFP in wild-type (left) and in low-dose *foxC1*dMO morphant embryos (right) at 48hpf. No differences in overall morphology was noted in low-dose morphants. **C.** Intersegmental vessels in wild-type (left) and low-dose *foxC1*dMO morphant (right) embryos at 48 hpf. **D.** Microangiography in wild-type (left) and low-dose *foxC1*dMO morphant embryos (right) at 4 dpf. Note the increased leakage of dye into the anterior chamber of *foxC1*dMO eyes.

NIH-PA Author Manuscript
NIH-PA Author Manuscript
NIH-PA Author Manuscript



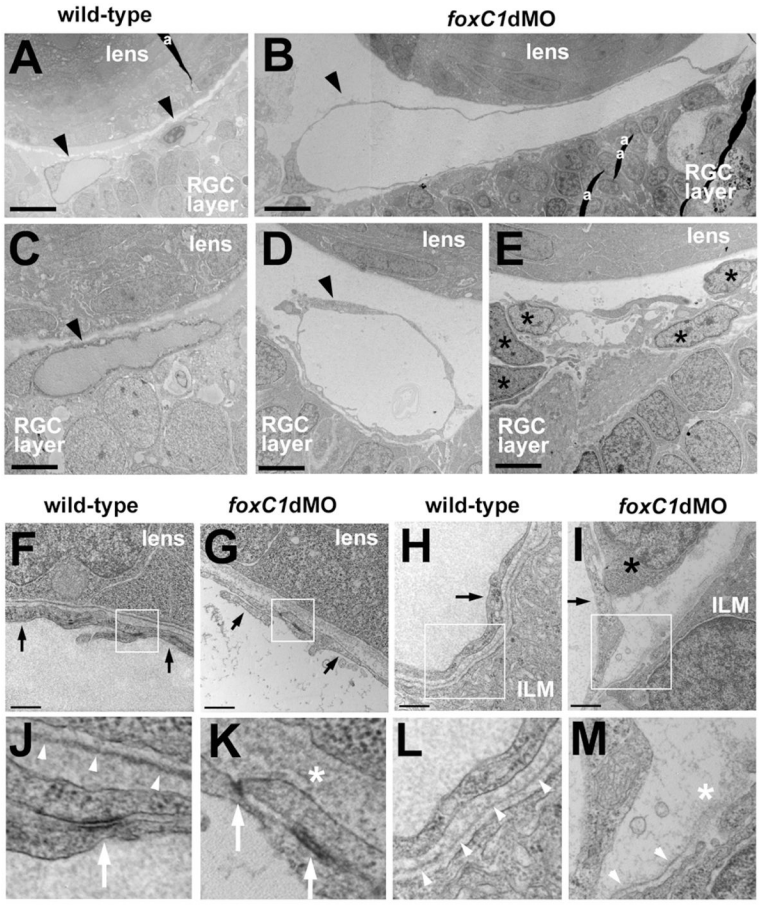


**Figure 6. Ultrastructure of hyaloid vasculature in 48hpf *foxC1*dMO embryos**

Hyaloid vascular endothelial cells (black arrowheads) in wild-type **(A, C)** and *foxC1*dMO eyes **(B, D).** In some *foxC1*dMO embryos, undifferentiated mesenchymal cells (**E**, black asterisks) occupied the space where vessels normally reside. Vascular endothelial cells (black arrows) associated with the basal surface of the lens cells in wild-type **(F)** or *foxC1*dMO embryos **(G)**. Vascular endothelial cells (black arrows) associated with the basal surface of the retina in wild-type **(H)** or *foxC1*dMO embryos **(I)**. Black asterisk in (I) indicates undifferentiated mesenchymal cell. Boxed areas indicate magnified regions below **(J–M)**. Basement membranes (white arrowheads) or disorganized extracellular matrix (white asterisk) associated with the lens cells (J,K) or the ILM of the retina (L,M). Note the discontinuous and disorganized basement membranes associated with *foxC1*dMO vascular cells. Bar equals 10 microns (A,B); 4 microns (C–E); 0.5 microns (F–I). RGC, retinal ganglion cell; ILM, inner limiting membrane of the retina; a, artifact (section fold).

NIH-PA Author Manuscript
NIH-PA Author Manuscript
NIH-PA Author Manuscript



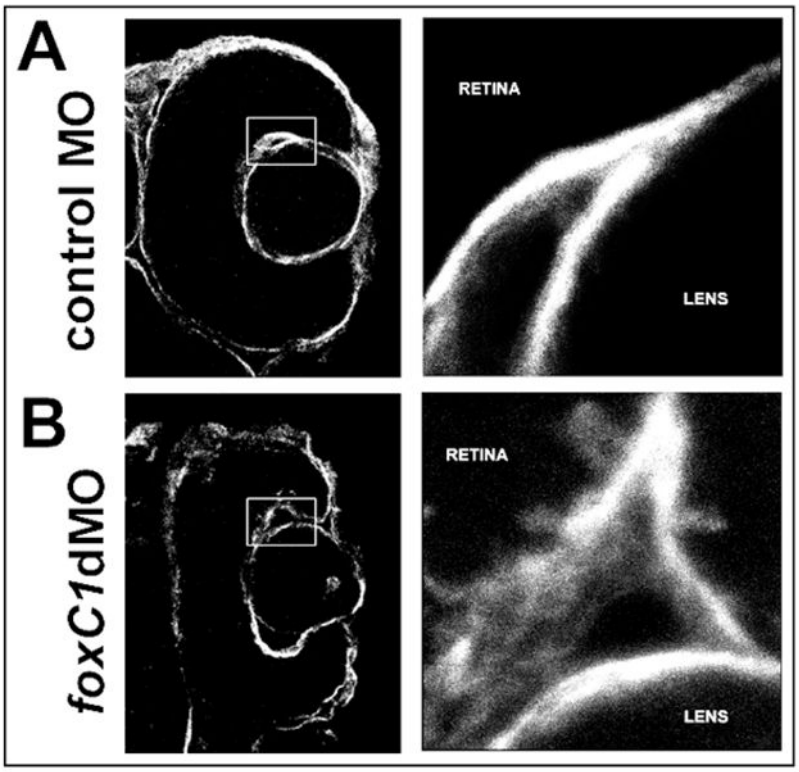


**Figure 7. Laminin-111 immunostaining in *foxC1*dMO eyes**

Immunostaining for Laminin-111 in the basement membranes of 48 hpf control morphant **(A)** and *foxC1*dMOs **(B)** eyes. Higher magnification of boxed inset shown on the right of each panel.

NIH-PA Author Manuscript
NIH-PA Author Manuscript
NIH-PA Author Manuscript



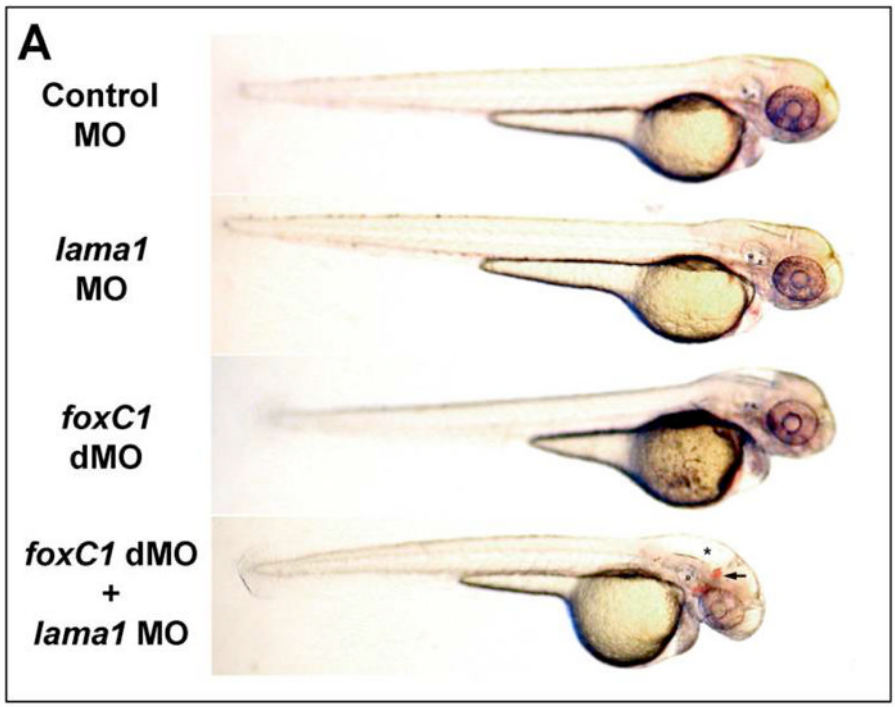


B

| | Control MO | *lama1* MO | *foxC1* dMO | *foxC1* dMO + *lama1* MO |
|---|---|---|---|---|
| n= | 128 | 122 | 171 | 182 |
| Blood Flow | 99% | 99% | 94% | 93% |
| Hemorrhage | 2% | 11% | 24% | 36% |
| Hydrocephaly | 2% | 18% | 21% | 43% |

**Figure 8. Effects of *lama1* loss on *foxc1*dMO phenotypes**

**A.** Mild phenotypes were found after low-dose knockdown of both *foxC1* and *lama1* (middle panels) as compared to controls (upper panel). Increased incidence hydrocephaly (asterisk) and hemorrhaging (arrow) was found after co-injection of these same doses of *foxC1* and *lama1* morpholinos (lower panel). **B.** Quantification of phenotypes described above. Data represents totals from three independent experiments.